Accepted Manuscript

A wet process for oxidation-absorption of nitric oxide by persulfate/calcium peroxide

Zhiping Wang, Yanguo Zhang, Zhongchao Tan, Qinghai Li

PII: S1385-8947(18)30959-8
DOI: https://doi.org/10.1016/j.cej.2018.05.145
Reference: CEJ 19161

To appear in: *Chemical Engineering Journal*

Received Date: 19 March 2018
Revised Date: 22 May 2018
Accepted Date: 24 May 2018

Please cite this article as: Z. Wang, Y. Zhang, Z. Tan, Q. Li, A wet process for oxidation-absorption of nitric oxide by persulfate/calcium peroxide, *Chemical Engineering Journal* (2018), doi: https://doi.org/10.1016/j.cej.2018.05.145

A wet process for oxidation-absorption of nitric oxide by persulfate/calcium peroxide

Zhiping Wang[a,c], Yanguo Zhang[a,c], Zhongchao Tan[b,c], Qinghai Li[a,c*]

[a]*Key Laboratory for Thermal Science and Power Engineering of Ministry of Education, Department of Energy and Power Engineering, Tsinghua University, Beijing 100084, PR China*

[b]*Department of Mechanical & Mechatronics Engineering, University of Waterloo, Ontario N2L 3G1, Canada*

[c]*Tsinghua University-University of Waterloo Joint Research Center for Micro/Nano Energy & Environment Technology, Tsinghua University, Beijing 100084, PR China*

Abstract

This study develops and evaluates a novel wet method for NO removal using a $Na_2S_2O_8/CaO_2$ solution. The effects of these two components both and alone in solution, $Na_2S_2O_8$ concentration, CaO_2 concentration, initial pH, reaction temperature, and the concentrations of NO and O_2 on NO removal efficiency were evaluated using a bubbling reactor. The combination of $Na_2S_2O_8$ and CaO_2 had a synergistic effect on NO removal efficiency. NO removal was effected by CaO_2 concentration, reaction temperature and the initial solution pH, while $Na_2S_2O_8$ concentration and O_2 concentration had little effect. The NO removal efficiency decreased linearly from 94.5 % to 75.1 % when the NO concentration increased from 139 to 559 ppm. The products were characterized using XRD、XPS and IC, and $CaSO_4 \cdot 2H_2O$, $NaNO_3$ and

* Corresponding author. Tel: +86 10 62773188, E-mail address: liqh@tsinghua.edu.cn (Q.H. Li).

$CaNO_3$ were found to be the main products. The EPR analysis showed that free radicals of $O_2^{\bullet-}$, $SO_4^{\bullet-}$ and •OH were the key species involved in the NO removal process. Finally, the corresponding reaction mechanisms were proposed.

Keywords: NO removal; $Na_2S_2O_8$; CaO_2; Free radical; EPR analysis

1. Introduction

Nitric oxide (NO) accounts for more than 90 % of NO_x emitted from coal-fired boilers and plays a key role in the formation of photochemical smog and acid rain [1]. Several denitration techniques have been developed to control emissions of NO_x. Recently, selective catalytic reduction (SCR) or selective non-catalytic reduction (SNCR) have been widely used in industrialization [2]. In order to meet the required standards of emission concentrations for SO_2 and NO_x (lower than 35 and 50 mg/m^3, respectively), SCR or SNCR have been used before wet desulfurization in coal-fired boilers. However, this "1+1" type of approach to desulfurization and denitration has many disadvantages, including its complex system, large footprint and high operating cost [3, 4]. These disadvantages can be addressed by simultaneous removal of NO_x and SO_2 in the same wet scrubber.

Unlike SO_2, NO is an insoluble gas. Therefore, it is much more difficult to remove with conventional wet scrubbing [5]. To convert NO into more easily removable soluble nitrogen oxides, reagents are added that include ozone (O_3) [6], hydrogen peroxide (H_2O_2) [7], chlorine dioxide (ClO_2) [8], potassium permanganate ($KMnO_4$) [9], sodium chlorite ($NaClO_2$) [10], sodium hypochlorite (NaClO) [11], sodium persulfate ($Na_2S_2O_8$) [12], Fe(II)EDTA and $Co(NH_3)_6^{2+}$) [13-14]. There is much interest

in hydrogen peroxide (H_2O_2) in particular because it is relatively low cost and does not produce secondary pollution. Cooper et al. [15] studied the injection of H_2O_2 into hot flue gases for NO emission control. At the optimum temperature of 500 °C, hydrogen peroxide can be thermally activated to generate active radicals including hydroxyl radical (•OH) and hydroperoxy radical (HO_2•). More than 90 % of NO can be effectively converted into soluble nitrogen oxides by these radicals of •OH and HO_2•. However, this gas-phase oxidation method has so far only been studied in the laboratory due to the limitations imposed by the high temperatures required.

Persulfate can be stimulated by heat [16], UV light [17], ultrasonic [18] or transition metals (Fe^{2+}, Co^{2+}, Cu^{2+}) [19, 20] to generate sulfate radical ($SO_4^{\bullet-}$) (Eqs. 1-2), which is an oxidant with a similar function to •OH. Adewuyi et al. [5, 12] studied the absorption-oxidation of NO and SO_2 by $Na_2S_2O_8$ aqueous solution in a bubbling reactor. Their results indicated that $Na_2S_2O_8$ can be activated to generate active $SO_4^{\bullet-}$ radical at 50 °C, which then reacts with H_2O to produce •OH radical. The reaction rate was very slow ($k[H_2O] < 2 \times 10^{-3}\ s^{-1}$), and so NO and SO_2 were mainly removed by $SO_4^{\bullet-}$ radical in the thermal excitation system of $Na_2S_2O_8$ aqueous solution. Block et al. [21] found that $SO_4^{\bullet-}$ and •OH radicals coexisted in the dual oxidation ($S_2O_8^{2-}/H_2O_2$) system owing to the significant synergistic relationship between $S_2O_8^{2-}$ and H_2O_2. In our previous studies [22, 23], we also showed that the combination of $S_2O_8^{2-}$ and H_2O_2 had a significant synergistic effect on NO removal. In addition, the NO removal efficiency under alkaline conditions was much higher than that under acidic or neutral conditions, reaching 80 % or higher for a long period of time under strongly alkaline

conditions adjusted by the addition of sodium hydroxide (NaOH). All these indicated that $S_2O_8^{2-}$ can be activated by strong alkalinity, heat and H_2O_2. This finding was consistent with the conclusions of Zhao et al [24].

$$S_2O_8^{2-} + \text{heat/UV/ultrasonic} \rightarrow 2SO_4^{\bullet-} \quad (1)$$

$$S_2O_8^{2-} + Me^{n+} \rightarrow SO_4^{\bullet-} + SO_4^{2-} + Me^{(n+1)+} \quad (2)$$

The problems of H_2O_2 instability and extra consumption of NaOH in the dual oxidation ($S_2O_8^{2-}$/H_2O_2) system can be solved by dissolving the solid oxidant CaO_2 in water for producing H_2O_2 and $Ca(OH)_2$ as described in Eq. 3 [25]. As well as a source of H_2O_2 (liberating a maximum of 0.47 g H_2O_2/g CaO_2 [25]), CaO_2 is also a strong alkali oxidant. This means it can activate $S_2O_8^{2-}$ and can therefore be used as an absorbent for the alkaline absorption of NO and SO_2. To the best of our knowledge, no study on wet desulfurization and denitration using the dual component of $S_2O_8^{2-}$/CaO_2 has yet been reported.

$$CaO_2 + H_2O \rightarrow H_2O_2 + Ca(OH)_2 \quad (3)$$

This study was aimed to understand the feasibility of simultaneous absorption of NO using $S_2O_8^{2-}$/CaO_2. Specifically, the effects on NO removal of single and dual component methods, $S_2O_8^{2-}$ concentration, CaO_2 concentration, the initial pH, the reaction temperature, NO concentration, and O_2 concentration were investigated in a bubbling reactor. In addition, the related mechanisms of NO removal by $S_2O_8^{2-}$ and CaO_2 were revealed by free radical detection. The results would contribute to the knowledge of simultaneous removal of NO_x and SO_2 in the same wet scrubber.

2. Experimental

2.1. Materials

Flue gases were simulated by mixing N_2 (99.999 %), O_2 (99.999 %), and NO mixed gas (1 %). All gases were purchased from Air Liquide Tianjin Co., Ltd. Sodium persulfate ($Na_2S_2O_8$, powder, 99 %), sulfuric acid (H_2SO_4, liquid, 98 %), sodium hydroxide (NaOH, pellets, 96 %) and anhydrous calcium chloride ($CaCl_2$, pellets, 96 %) were supplied by Sinopharm Chemical Reagent Beijing Co., Ltd. All reagents used in this experiment were analytically pure. The calcium peroxide (CaO_2) powder (70 %) used was chemically pure and obtained from Shandong Western Chemical Industry Co., Ltd.

2.2. Experimental Procedure

Fig. 1 shows the experimental setup used in this study. It consisted of four parts, a simulated flue gas generation system, a bubble column reactor with an inner diameter of 75 mm and a height of 300 mm, a flue gas analysis system and a tail gas absorption system. The NO, O_2 and N_2 (Fig. 1, 1-3) had their flow rates measured by mass flowmeters (Fig. 1, 4) before being mixed in a surge flask (Fig. 1, 5). Concentrations of NO and O_2 were adjusted by diluting with N_2. The flow rate of the simulated flue gas was kept at 2 L/min.

All experiments were conducted at temperatures between 15-70 °C. The temperature was controlled by the digital thermostat water bath (Fig. 1, 9) (HWSH, ±0.1 °C, Shanghai Tian Heng Instrument co., Ltd). For a typical test, the bubble column reactor was first filled with 600 mL of water and heated to the required temperature. Sodium persulfate and calcium peroxide solutions were added into the

reactor until the total liquid volume reached 800 mL. The pH of the solution was adjusted by adding 3 mol/L H_2SO_4 or 2 mol/L NaOH solution into the reactor. When the liquid phase was ready, the simulated flue gas was passed through the bubbling reactor, the surge flask (Fig. 1, 10), the drying tube (Fig. 1, 11) containing anhydrous $CaCl_2$ used for the removal of moisture in the simulated flue gas, and finally through another surge flask (Fig. 1, 14) before entering the flue gas analyzer.

The direction of simulated flue gas flow was controlled by a 3-way valve (Fig. 1, 6). The inlet and outlet concentrations of NO_x and O_2 were measured by the ecom-J2KN flue gas analyzer (German RBR Measurement Technology Co., LTD). The pH of the reaction solution was measured before and after each test with a digital pH meter (PHS-3C, E-201F of electrode assembly type, ±0.01, Shanghai Leici Co., LTD). The tail gas was further cleaned by the exhaust gas absorption unit (Fig. 1, 17) before entering the fume hood (Fig. 1, 18).

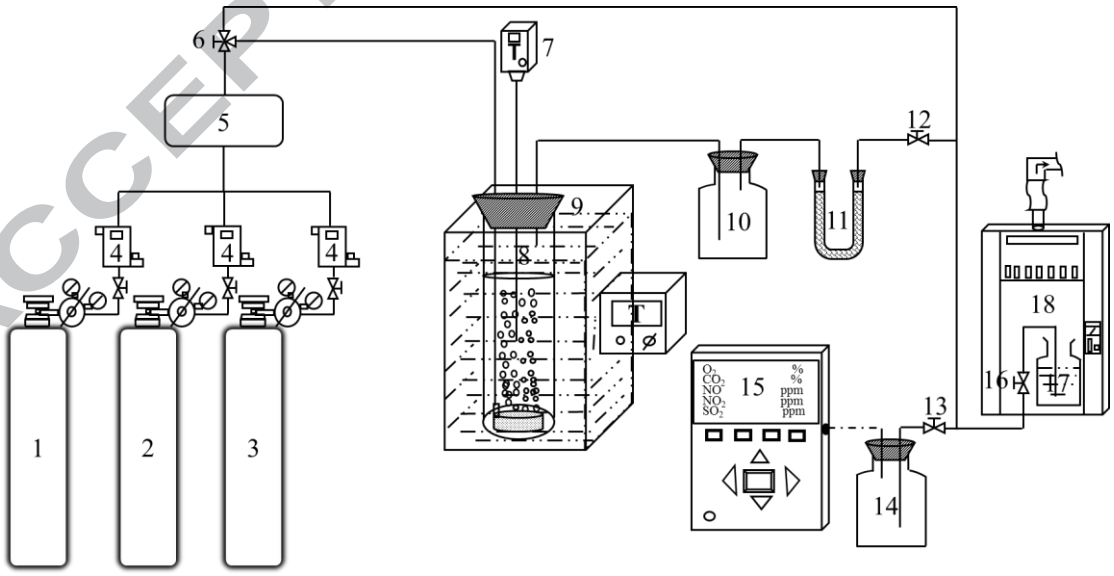

1-Nitric oxide cylinder; 2-Oxygen cylinder; 3-Nitrogen cylinder; 4-Mass flowmeter; 5- Surge flask; 6-3-way valve; 7-Electronic thermometer; 8-Bubble column reactor;

9-Thermostat water bath; 10-Surge flask; 11-Dryer; 12,13,16-Two-way valve; 14-Surge flask; 15-Flue gas analyzer; 17- Exhaust gas absorption unit; 18-Fume hood.

Fig. 1. Schematic diagram of the experimental setup.

2.3. Data Analysis

The ions in the spent scrubbing solution were analyzed with a Dionex ICS 1000 ion chromatography system under the following chromatographic conditions: ion pac AS11-HC capillary column (4 × 250 mm), eluent (2 mmol/L NaOH), injection volume (25 μL), column temperature (303 K), flow rate (1.0 mL/min) and automatic regeneration suppression system (60 mmol H_2SO_4 and H_2O). The crystalline structure of fresh and spent solid absorbents was analyzed by X-ray diffraction (XRD, D8 ADVANCE type, BRUKER-AXS in Germany) (60 kV and 50 mA) with a Ni-Filtered Cu Kα, with a scanning 2θ range of 5^0 to 90^0 and a step size of 0.02. The fresh and spent solids were analyzed by X-ray photoelectron spectroscopy (XPS, PHI Quantera SXM Scanning ESCA Microprobe (Physical Electronics), Ulvac-Phi Inc in Japan) with a hemispherical detector operated at a constant pass energy (PE=55 eV) using Al Kα radiation (1486.6 eV). All binding energies were referenced to C 1s line at 284.8 eV. Active free radical species were detected with an electron spinresonance (EPR) spectrometer (JES-FA200) using 5,5-dimethyl-1-pyrrolidine N-oxide (DMPO) (99 %, Sigma) as a spin trap agent.

The inlet concentrations of NO_x and O_2 were measured immediately upstream of the gas inlet. The outlet concentrations of NO_x and O_2 from the bubble column reactor were continuously monitored and recorded. Each measurement lasted for 90 minutes,

and the mean concentration within the 90 minutes was used for the calculation of removal efficiency. When the mixed gas was bubbled through the reactor, NO reacted with the $S_2O_8^{2-}/CaO_2$ solution. The corresponding NO removal efficiency was calculated by:

$$\eta_{NO}(\%) = \frac{NO_{inlet} - NO_{outlet}}{NO_{inlet}} \times 100 \quad (4)$$

where η_{NO} is the removal efficiency of NO, NO_{inlet} and NO_{outlet} are the NO concentrations in the inlet and outlet gas.

3. Results and Discussions

3.1. Stability of the dual component of $Na_2S_2O_8/CaO_2$

Experiments were conducted with the pH changes of different $Na_2S_2O_8/CaO_2$ solutions over time at room temperature and atmosphere pressure to determine the stability of $Na_2S_2O_8/CaO_2$ solution. The corresponding results are shown in Fig. 2. 0.1 mol/L $Na_2S_2O_8$ solution was acidic due to the hydrolysis of $Na_2S_2O_8$ via Eq. 5 [5], and exhibited negligible change in pH over time, likely because of the very slow hydrolysis of $Na_2S_2O_8$ at room temperature and atmosphere pressure [26]. 0.22 mol/L CaO_2 solution was strongly alkaline and exhibited a slow increase in pH over time because of the slow release of $Ca(OH)_2$ caused by the dissolution of CaO_2 in water via Eq. 3 [25, 27]. The change in pH of different $Na_2S_2O_8/CaO_2$ solutions was not large enough to suggest instability. We therefore consider $Na_2S_2O_8/CaO_2$ solution to be stable at room temperature and atmosphere pressure.

$$2S_2O_8^{2-} + 2H_2O \rightarrow 4HSO_4^- + O_2 \quad (5)$$

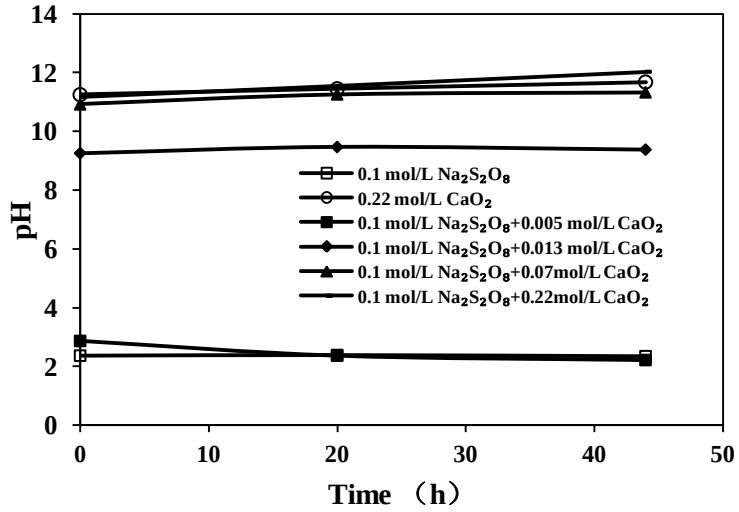

Fig. 2. The pH changes of different $Na_2S_2O_8/CaO_2$ solutions vs. time.

3.2. Effects of single and dual component on NO removal

3.2.1 Effect of CaO_2

In order to verify the synergistic effects of $Na_2S_2O_8$ and CaO_2, the effects of each, both alone (single component) and together (dual component) on NO removal performance were analyzed at 55.5 °C. Fig. 3 shows that NO removal efficiency was about 10 % when using CaO_2 alone. This confirmed our expectations that H_2O_2 released from CaO_2 has weak oxidation capacity due to its low oxidation reduction potential (E^{θ} (H_2O_2) =1.77 V). As shown in Fig. 3, NO removal efficiency decreased from 21 % to 6 % for the reaction time of 4000 s. One reason for the decrease of NO removal efficiency with time might be that as the reaction proceeded, the main oxidant H_2O_2 released from CaO_2 was gradually consumed to remove NO. In addition, the pH of the single CaO_2 solution increased from 10.98 to 11.54 for the reaction time of 4000 s. Zhang et al. [27] found that the generation rate of H_2O_2 from CaO_2 slowed down with the increase of pH, which may also explain the observed decline in removal efficiency. O_2 was not detected in the NO removal process when CaO_2 was

the only component. This is because the release of O_2 through the decomposition of H_2O_2 (See Eq. 6) and the dissolution of CaO_2 in water (See Eq. 7) were inhibited by the increase of alkalinity [27]. In addition, the released O_2 was fully involved in the oxidation process of nitrogen oxides.

$$2H_2O_2 \rightarrow 2H_2O + O_2 \quad (6)$$

$$2CaO_2 + 2H_2O \rightarrow 2Ca(OH)_2 + O_2 \quad (7)$$

3.2.2 Effect of $Na_2S_2O_8$

Fig. 3 shows that the NO removal efficiency reached approximately 20 % when $Na_2S_2O_8$ was the only component. $Na_2S_2O_8$ can be thermally decomposed into $SO_4^{\bullet-}$ at 55.5 °C (See Eq. 8). Water can consume $SO_4^{\bullet-}$ at all pH levels to produce •OH as described in Eq. 9, but the rate of this reaction is very slow ($k[H_2O] < 2 \times 10^{-3}\ s^{-1}$) [5]. $SO_4^{\bullet-}$ was the main oxidant due to its high oxidation reduction potential of $E^{\theta}(SO_4^{\bullet-})$ =2.60 V. NO removal efficiency decreased from 30 % to 13 % once the reaction time reached 4000 s because $Na_2S_2O_8$ was constantly consumed during the reaction, leading to a decrease in the generation of $SO_4^{\bullet-}$. O_2 concentrations in the outlet flue gas remained at 0 % with the reaction time of 4000 s in the NO removal process with single $Na_2S_2O_8$. This could be because the O_2 released from hydrolysis of $Na_2S_2O_8$ (See Eq. 5) was fully involved in the oxidation process of nitrogen oxides.

$$S_2O_8^{2-} \xrightarrow{\text{heat}} 2SO_4^{\bullet-} \quad (8)$$

$$SO_4^{\bullet-} + H_2O \rightarrow \bullet OH + SO_4^{2-} + H^+ \quad (9)$$

3.2.3 Effect of dual components

Fig. 3 also shows that the denitration performance of the combined dual

component $Na_2S_2O_8/CaO_2$ solution were much better than that of systems with $Na_2S_2O_8$ or CaO_2 only. The NO removal efficiency could remain at 70 % or higher when both $Na_2S_2O_8$ and CaO_2 were present. These results indicate that the combination of $Na_2S_2O_8$ and CaO_2 has great synergistic effects on the removal of NO. As seen in Fig. 3, the NO removal efficiency curve for the reaction time of 6300 s first dropped, then rose, and finally remained stable. This is because $Na_2S_2O_8$ reacted with H_2O_2 to generate $SO_4^{\bullet-}$ and $HO_2\bullet$ via Eqs. 10-11 [23, 26]. $HO_2\bullet$ quickly reacted with OH^- to produce $O_2^{\bullet-}$ (See Eq. 12) [28]. $Na_2S_2O_8$ was activated by OH^- to generate $SO_4^{\bullet-}$ and $O_2^{\bullet-}$ (See Eqs. 13-14) [29]. NO removal efficiency decreased once the reaction time reached 3000 s because of the constant consumption of these reactive radicals by NO. The pH of the dual component $Na_2S_2O_8/CaO_2$ increased from 10.26 to 11.72 once the reaction time reached 6300 s. The resulting alkaline conditions caused the formation of •OH radicals via Eq. 15 [29]. These are more reactive than $SO_4^{\bullet-}$ and $O_2^{\bullet-}$. As a result, NO removal efficiency increased and finally remained stable after the reaction time passed 3000 s. The O_2 concentration first fell, then rose, and then decreased to 0 at 6300 s. The propagation and scavenging reactions among the excess $SO_4^{\bullet-}$, •OH and $O_2^{\bullet-}$ (See Eqs. 16-17) [29] increased the O_2 concentration for the time from 3000s to 4000s. The constant consumption of O_2 released from chemical reactions between $Na_2S_2O_8$ and CaO_2 during the oxidation process of nitrogen oxides reduced the O_2 concentration after 6300 s.

$$S_2O_8^{2-} \xrightarrow{\text{heat}} 2SO_4^{\bullet-} \quad (10)$$

$$SO_4^{\bullet-} + H_2O_2 \rightarrow H^+ + SO_4^{2-} + HO_2\bullet \quad (11)$$

$$HO_2 \bullet \xrightarrow{OH^-} O_2^{\bullet-} + H^+ \quad (12)$$

$$S_2O_8^{2-} + 2H_2O \xrightarrow{OH^-} HO_2^- + 2SO_4^{2-} + 3H^+ \quad (13)$$

$$S_2O_8^{2-} + HO_2^- \rightarrow SO_4^{\bullet-} + SO_4^{2-} + H^+ + O_2^{\bullet-} \quad (14)$$

$$SO_4^{\bullet-} + OH^- \rightarrow SO_4^{2-} + \bullet OH \quad (15)$$

$$SO_4^{\bullet-} + O_2^{\bullet-} \rightarrow SO_4^{2-} + O_2 \quad (16)$$

$$\bullet OH + O_2^{\bullet-} \rightarrow OH^- + O_2 \quad (17)$$

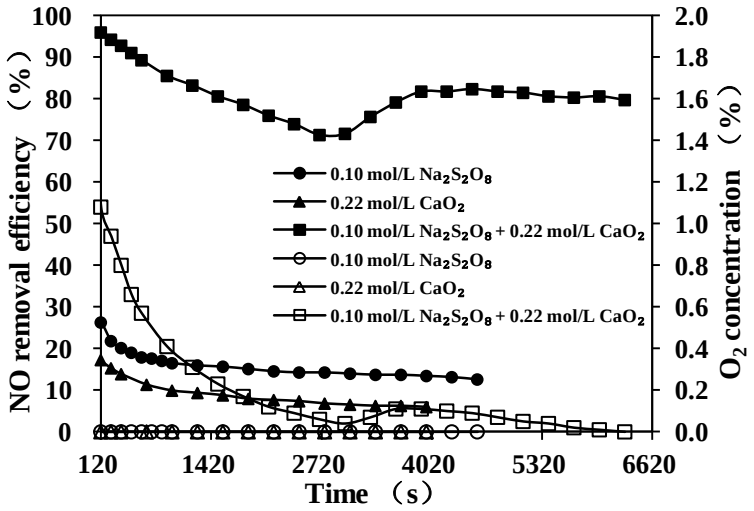

Fig. 3. Effects of single and dual component on NO removal (Reaction temperature= 55.5 ℃; total gas flow= 2 L/min; NO concentration= 345 ppm; O_2 concentration= 0 %) (Full symbol — NO removal efficiency; Void symbol — O_2 concentration).

3.3. Effects of CaO_2 and $Na_2S_2O_8$ concentration on NO removal

The effects of CaO_2 concentration on NO removal efficiency were analyzed (Fig. 4). With an increase of CaO_2 concentration from 0.005 mol/L to 0.215 mol/L, the NO removal efficiency increased from 18.3 % to 82.6 %. When CaO_2 concentration doubled from 0.215 mol/L to 0.413 mol/L, the efficiency increased by only 3 %. The increase of CaO_2 concentration improved the yields of $SO_4^{\bullet-}$, $O_2^{\bullet-}$ and •OH free radicals (See Eqs. 10-15), thereby enhancing the efficiency of NO removal. However,

the scavenging reactions of excess free radicals generated by excess CaO_2 competed with the reactions among free radicals with NO (See Eqs. 16-20). The changes of NO removal efficiency curves over time for low CaO_2 concentrations (i.e. 0.005 and 0.014 mol/L) were different from those for higher CaO_2 concentrations (from 0.073 to 0.430 mol/L). The pH of 0.005 mol/L CaO_2 concentration decreased from 3.0 to 2.51 after the reaction had been in progress for 4980 s, while that of 0.014 mol/L CaO_2 concentration decreased from 8.6 to 8.41 after the reaction had been in progress for 5520 s. The presence of $SO_4^{\bullet-}$ radical generated by the thermal activation of $Na_2S_2O_8$ was attributed to the release of small amounts of H_2O_2 and $Ca(OH)_2$ from CaO_2 at low concentration. At higher CaO_2 concentrations (from 0.073 to 0.430 mol/L), the changes of NO removal efficiency curve over time were almost similar attributing for the similar changes of pH of dual component of $Na_2S_2O_8/CaO_2$ from 10.01 to 11.35, from 10.80 to 11.80 and from 10.87 to 11.83 with the reaction times of 5400 s, 6300 s and 6420 s respectively, when the corresponding CaO_2 concentrations were 0.073, 0.215 and 0.430 mol/L respectively.

$$\bullet OH + \bullet OH \rightarrow H_2O_2 \quad (18)$$

$$SO_4^{\bullet-} + SO_4^{\bullet-} \rightarrow S_2O_8^{2-} \quad (19)$$

$$SO_4^{\bullet-} + \bullet OH \rightarrow HSO_5^{-} \quad (20)$$

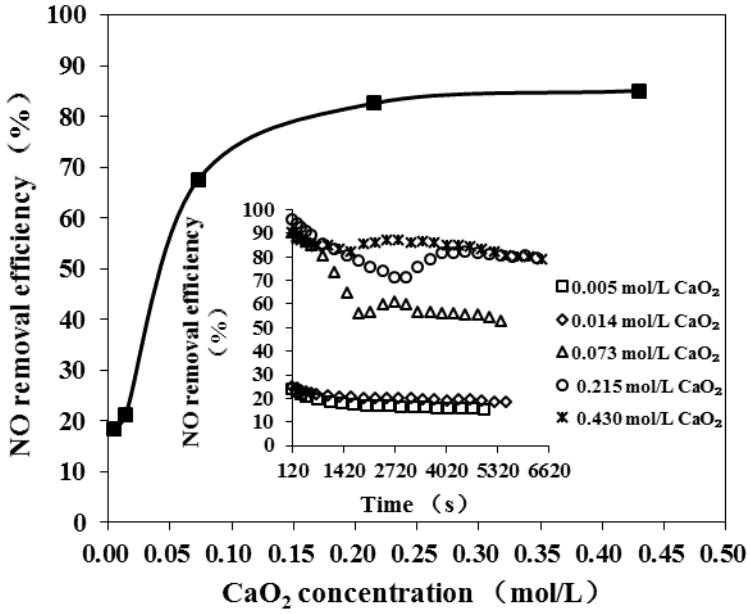

Fig. 4. Effects of CaO_2 concentration on NO removal efficiency (Reaction temperature = 55.5 °C; total gas flow= 2 L/min; NO concentration= 345 ppm; O_2 concentration= 0 %; $Na_2S_2O_8$ concentration= 0.1 mol/L).

The effects of $Na_2S_2O_8$ concentration on NO removal efficiency are shown in Fig. 5. NO removal efficiency clearly increased when $Na_2S_2O_8$ concentration increased from 0.03 mol/L to 0.05 mol/L, and increased slightly when $Na_2S_2O_8$ concentration changed from 0.05 mol/L to 0.14 mol/L. The increase in $Na_2S_2O_8$ concentration improved the yields of $SO_4^{\bullet-}$, $O_2^{\bullet-}$ or •OH free radicals (See Eqs. 10-15), and consequently enhanced the removal efficiency of NO. However, the scavenging reactions of excess free radicals generated by the excess $Na_2S_2O_8$ would compete for the free radicals which react with NO (See Eqs. 16-20). NO removal efficiency for the $Na_2S_2O_8$ concentration of 0.03 mol/L declined constantly until 5400s. This was because there was too little $SO_4^{\bullet-}$ produced from $Na_2S_2O_8$ to generate $O_2^{\bullet-}$ and •OH. Therefore, $SO_4^{\bullet-}$ was fully involved in the oxidation of NO. The changes in NO removal efficiency over time followed a similar trend at higher $Na_2S_2O_8$

concentrations (from 0.05 to 0.14 mol/L). The pH of dual component of $Na_2S_2O_8/CaO_2$ solutions changed from 10.98 to 11.88, from 10.80 to 11.78, from 10.76 to 11.80 and from 10.0 to 11.72 for the reaction times of 6240 s, 6000 s, 6000 s and 5820 s at higher $Na_2S_2O_8$ concentrations of 0.05, 0.08, 0.10 and 0.14 mol/L, respectively.

$Na_2S_2O_8$ concentration had relatively little effect on NO removal efficiency when compared with CaO_2 concentration. Considering the costs and denitration performances, CaO_2 concentration of 0.215 mol/L and $Na_2S_2O_8$ concentration of 0.10 mol/L were recommened as the optimal concentration.

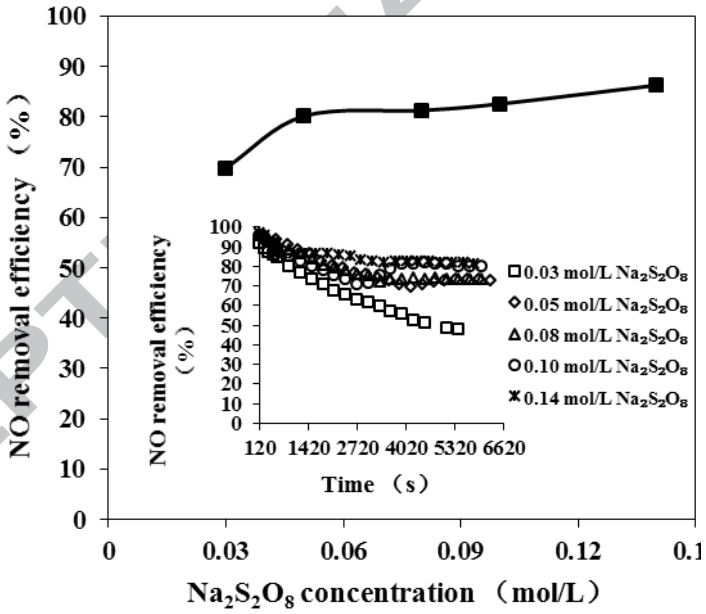

Fig. 5. Effects of $Na_2S_2O_8$ concentration on NO removal (reaction temperature= 55.5 ℃; total gas flow= 2 L/min; NO concentration= 345 ppm; O_2 concentration= 0 %; CaO_2 concentration= 0.215 mol/L).

3.4. Effects of temperature and pH on NO removal

Temperature affects the mass transfer rate of the chemicals of concern [30], while pH has obvious effects on the forms and oxidation-absorption potentials of the active

species in the solution [31]. The effects of temperature on NO removal efficiency are shown in Fig. 6. NO removal efficiency increased from 15.9 % to 82.6 % when the temperature increased from 18.0 ℃ to 55.5 ℃. The increase leveled off when the temperature changed from 55.5 ℃ to 65.5 ℃. These results were similar to those for dual oxidant ($Na_2S_2O_8/H_2O_2$) system in our previous studies [23]. The production of $SO_4^{\bullet-}$ increased with the increase of temperature. Liu et al. [32] also showed that the yields of $SO_4^{\bullet-}$ increased as the activation temperature increased from 25 to 75 ℃. In addition, the solubility of NO decreased with the increase of temperature. The change of NO removal efficiency at 18.0 ℃ over time was different from those at higher temperatures in the range of 35.5-65.5 ℃. $Na_2S_2O_8$ can not be thermally activated at 18.0 ℃ to produce $SO_4^{\bullet-}$ and $O_2^{\bullet-}$, and so NO was removed mainly by the $Na_2S_2O_8$ and H_2O_2 released by CaO_2 at 18.0 ℃.

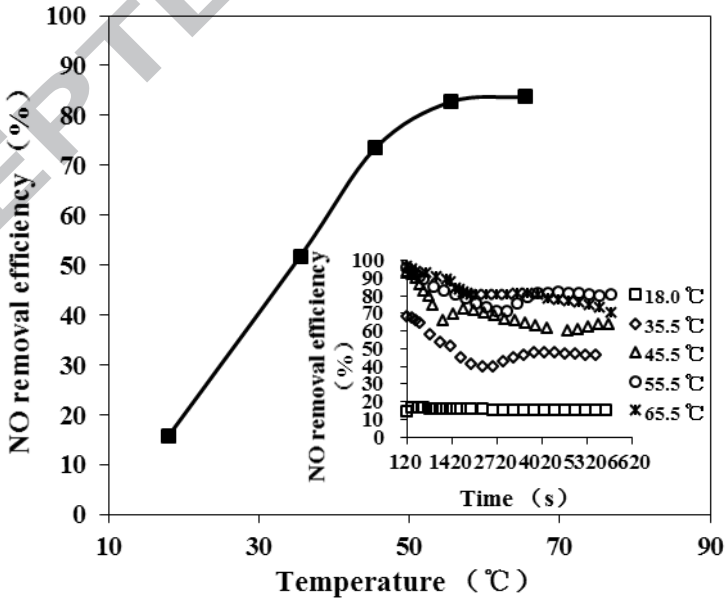

Fig. 6. Effects of temperature on NO removal (total gas flow= 2 L/min; NO concentration= 345 ppm; O_2 concentration= 0 %; CaO_2 concentration= 0.215 mol/L; $Na_2S_2O_8$ concentration= 0.1 mol/L; pH= 10.80).

The effects of pH on NO removal efficiency are shown in Fig. 7. NO removal efficiency increased from 7.8 % to 83.0 % when pH increased from 2.25 to 9.05, but there was little effect on the NO removal efficiency at pH levels higher than 9.05. The yields of H_2O_2 from CaO_2 increased with the addition of a small amount of H_2SO_4, thereby increasing the yields of $SO_4^{\bullet-}$, $O_2^{\bullet-}$ and •OH free radicals (See Eqs. 10-15). Northup et al. [25] also verified that the yields of H_2O_2 and the dissolution rate of CaO_2 increased with the decrease of pH. However, the generation of white turbid $CaSO_4$ from the consumption of CaO_2 by H_2SO_4 (via Eq. 21) increased as the amount of H_2SO_4 increased. It can be seen from Fig.8 that the white turbid $CaSO_4$ mainly existed in the dual component $Na_2S_2O_8/CaO_2$ solution at pH 2.25, which had little effect on the oxidation and absorption of NO. When pH increased from 10.80 to 12.34 with the addition of NaOH solution, NO removal efficiency decreased from 82.6 % to 75.5 %. The dissolution rate of CaO_2 was inhibited with the addition of NaOH solution, thereby decreasing the yields of $SO_4^{\bullet-}$, $O_2^{\bullet-}$ and •OH free radicals (See Eqs. 10-15) due to the decrease of H_2O_2 produced from CaO_2. The existence of SO_2 in flue gas would therefore be beneficial to the removal of NO in the dual component of $Na_2S_2O_8/CaO_2$ solution.

$$H_2SO_4 + CaO_2 \rightarrow CaSO_4 + H_2O \quad (21)$$

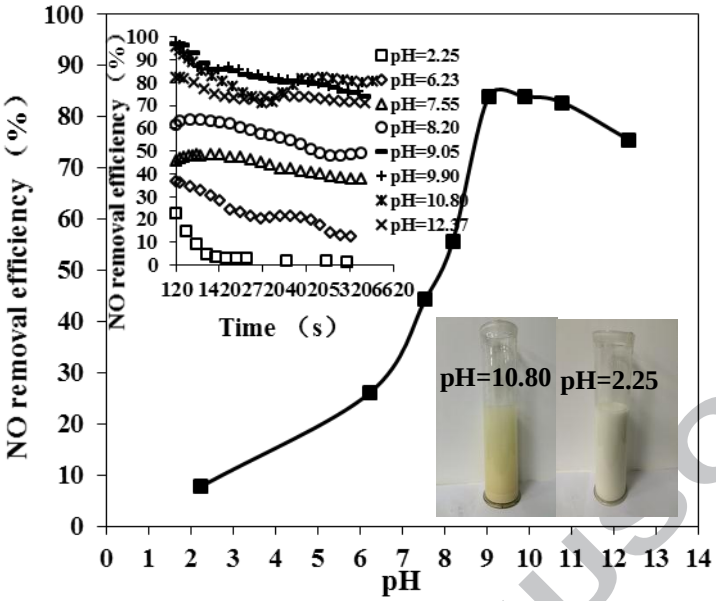

Fig. 7. Effects of pH on NO removal (total gas flow= 2 L/min; NO concentration= 345 ppm; O_2 concentration= 0 %; CaO_2 concentration= 0.215 mol/L; $Na_2S_2O_8$ concentration= 0.1 mol/L; temperature= 55.5 °C).

3.5. Effects of NO and O_2 concentrations on NO removal

For coal-fired boilers, the emissions of NO_x and O_2 depend on the properties of the coal used and the combustion conditions in the furnace. As shown in Fig. 8, NO removal efficiency almost linearly decreased from 94.5 % to 75.1 % as the NO concentration increased from 139 ppm to 559 ppm. At a lower NO concentration (139 ppm), the yields of $SO_4^{\bullet-}$, $O_2^{\bullet-}$ and •OH free radicals (Eqs. 10-15) were adequate to sustain an NO removal efficiency level of 90 % or higher for the reaction time of 5940 s. At higher NO concentrations (205, 279, 345, 415 and 559 ppm), NO removal efficiency decreased with the increase of NO concentration, perhaps because of the decrease of the ratio of reactive radicals to NO. However, the changes of NO removal efficiencies at all NO concentrations over time followd similar trends.

As shown in Fig. 9, the NO removal efficiency decreased a little and then

increased as the O_2 concentration increased from 0 % to 8 %. While the free radicals might be captured by O_2 [33], the oxidation and absorption of NO was also promoted by O_2 (See Eqs. 22-23). The effect of O_2 concentration on NO removal efficiency was less obvious. In addition, the changes in NO removal efficiency at all O_2 concentrations over time were similar to each other.

$$NO + O_2 \rightarrow NO_2 \quad (22)$$

$$NO + NO_2 + O_2 \rightarrow HNO_3 \quad (23)$$

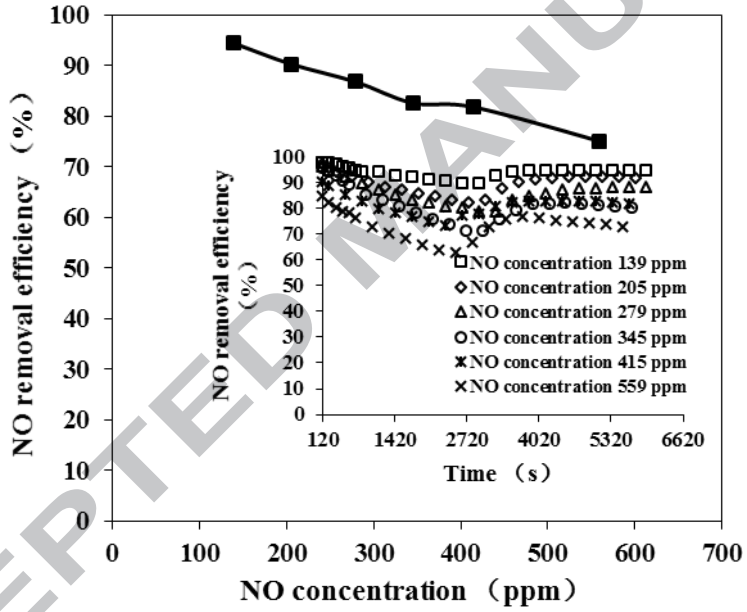

Fig. 8. Effects of NO concentration on NO removal efficiency (total gas flow= 2 L/min; O_2 concentration= 0 %; CaO_2 concentration= 0.215 mol/L; $Na_2S_2O_8$ concentration= 0.1 mol/L; temperature= 55.5 °C; pH= 10.80).

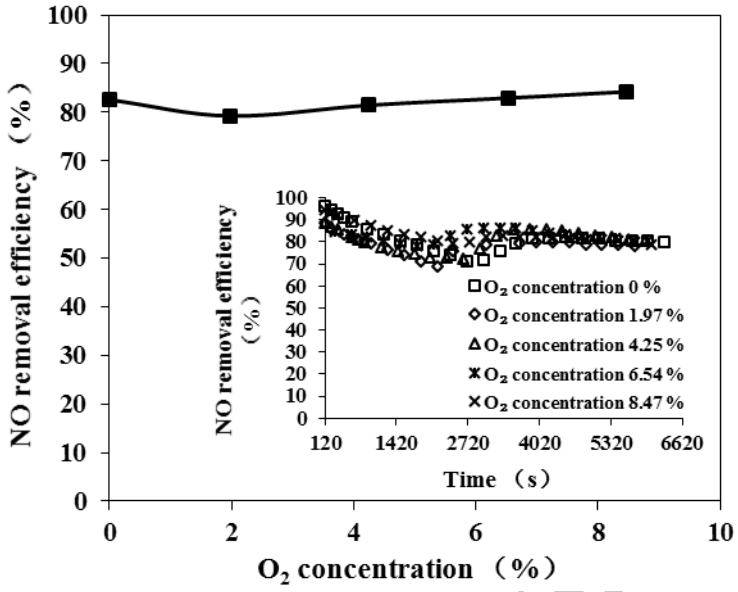

Fig. 9. Effects of O_2 concentration on NO removal efficiency (total gas flow= 2 L/min; NO concentration= 345 ppm; CaO_2 concentration= 0.215 mol/L; $Na_2S_2O_8$ concentration= 0.1 mol/L; temperature= 55.5 °C; pH= 10.80).

3.6. Reliability and replicability of the experiments

In order to verify the reliability and replicability of the experimental results, five parallel experiments were carried out under the determined optimal conditions. The $Na_2S_2O_8$ concentration was 0.1 mol/L, CaO_2 concentration 0.215 mol/l, solution pH 10.80, reaction temperature 55.5 °C, O_2 concentration 0 %, total gas flow 2 L/min and NO concentration 345 ppm. The results are shown in Fig. 10 and Table 1. The standard error of 2.66 % indicated a good degree of repeatability. Thus the experimental results were deemed to be reliable and to provide useful information for future industrial application.

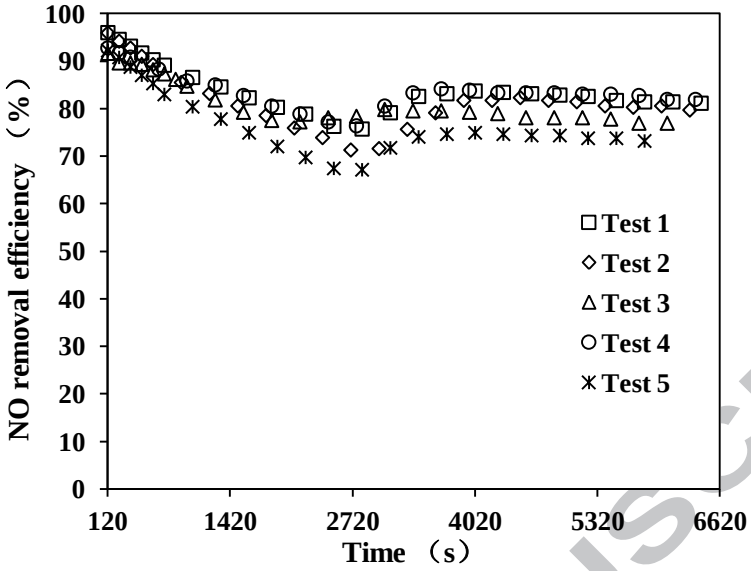

Fig. 10. Five parallel tests for NO removal with dual component of $Na_2S_2O_8/CaO_2$ solution.

Table 1 The results of five parallel tests for NO removal with dual component of $Na_2S_2O_8/CaO_2$ solution

Test	1	2	3	4	5	Average	Standard error
NO removal efficiency (%)	84.7	82.6	82.2	84.1	77.9	82.3	2.66

3.7. Reaction mechanisms

The XRD analysis for fresh CaO_2 and spent absorbents were conducted and the results are shown in Fig. 11. CaO_2 was identified as the main chemical component of the fresh 70 % CaO_2 powder, with possible $Ca(OH)_2$ and $CaCO_3$. $CaSO_4 \cdot 2H_2O$ was the main solid phase product throughout the oxidation and absorption of NO by $Na_2S_2O_8/CaO_2$. Unreacted $Ca(OH)_2$ was the main solid phase product generated by the hydrolysis of CaO_2, along with unreacted CaO_2. There were no obvious spectra

indicating presence of $NaNO_3$, $NaNO_2$, Na_2SO_4 and $Ca(NO_3)_2$. This might be because these molecules existed in the liquid phase.

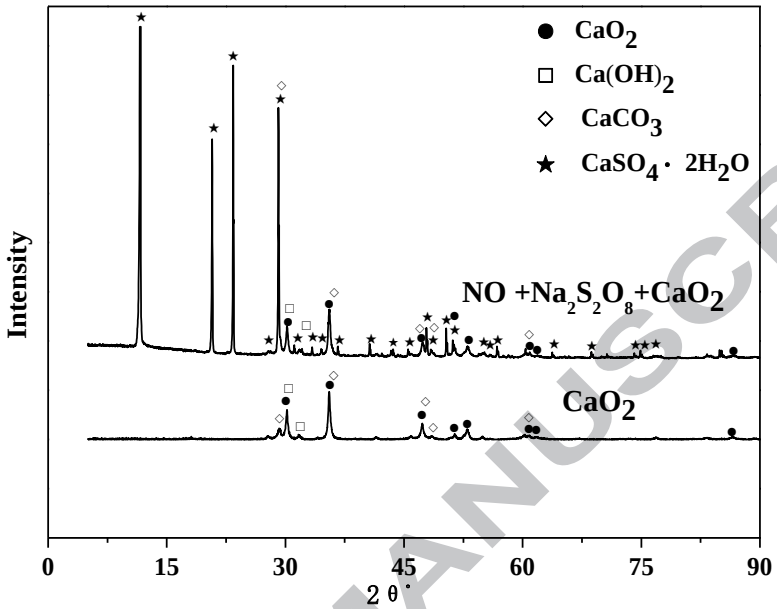

Fig. 11. XRD analysis results for the fresh CaO_2 and spent $Na_2S_2O_8/CaO_2$ absorbents.

XPS analysis of the solid $Na_2S_2O_8/CaO_2$ absorbent and IC analysis of liquid phase ion products were carried out to determine the elemental oxidation states of the generated species in solid and liquid phases. The results shown in Fig. 12 and Fig. 13 showed the photoelectron peak of O 1s appeared at the binding energy of 531.7 eV. This can be divided into four individual peaks at 530.7, 531.6, 532.1 and 532.4 eV corresponding to different oxygen-containing species, such as 530.7 eV for CO_3^{2-}, 531.6 eV for OH^-, 532.1 eV for SO_4^{2-}, and 532.4 eV for O_2^{2-}. The photoelectron peak of S 2p appeared at the binding energy of 168.6 eV, indicating the formation of SO_4^{2-}, which was consistent with the XPS results of O 1s. The spectrum of C 1s can be considered as two peaks at 285.1 and 289.2 eV, indicating the formation of C-C bonds and CO_3^{2-}, respectively. This was consistent with the XPS results of O 1s. There was no photoelectron peak at N 1s, indicating that there were no N-containing species in

the solid phase of the spent CaO_2 absorbents, although it did exist in the liquid phase. This observation was consistent with the XRD results. As shown in Fig. 13, NO_3^-, SO_4^{2-} and NO_2^- were detected in the NO removal system with the dual component of $Na_2S_2O_8/CaO_2$, but the amount of NO_2^- was negligible compared with that of NO_3^{2-}. SO_3^{2-} was not detected in the NO removal system with the dual component of $Na_2S_2O_8/CaO_2$.

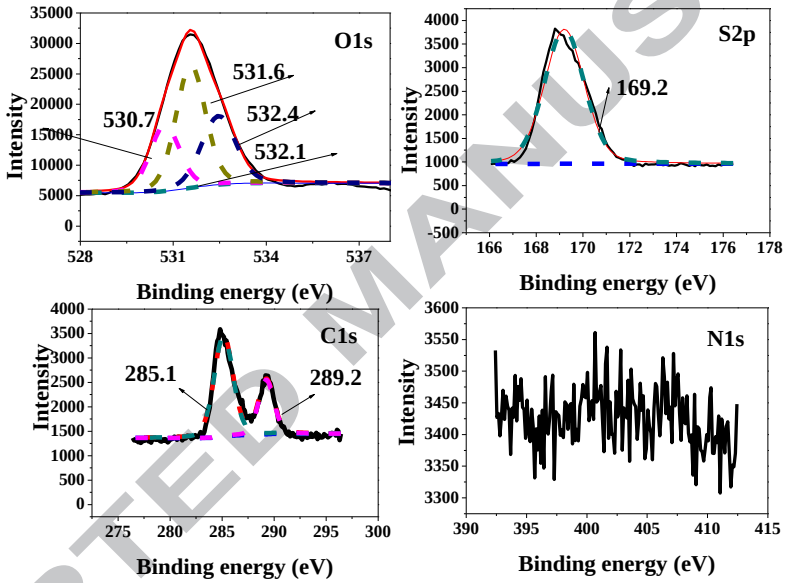

Fig.12. XPS spectra of spent $Na_2S_2O_8/CaO_2$ absorbents.

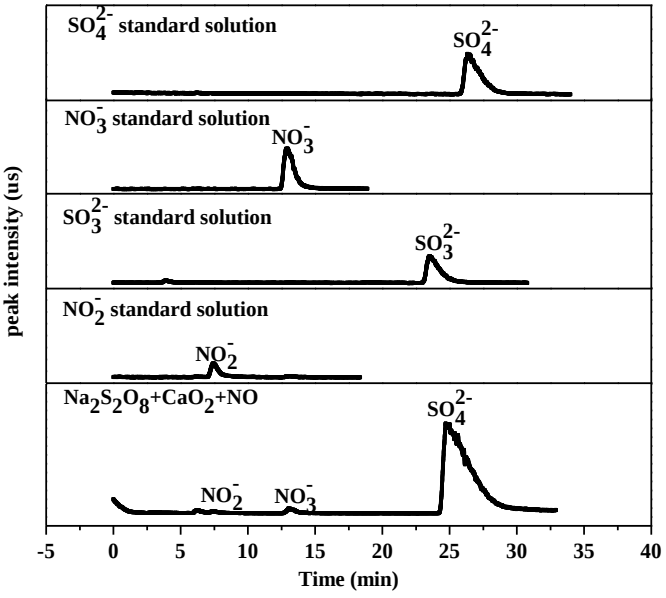

Fig.13. IC patterns of mixed standard solution and spent $Na_2S_2O_8/CaO_2$ solution.

Electron spin resonance (EPR) spectroscopy combined with DMPO was used to identify the reactive species involved in the reactions of the dual component of $Na_2S_2O_8/CaO_2$ solution at different times. The results are shown in Fig. 14. These hyperfine splitting constants of radical adducts (A_N=14.41 and A_H=9.94) were consistent with the data in literature [29, 34, 35]. The EPR peaks of $O_2^{\bullet-}$ radical were evident for the reaction times of 1 min, 5 min and 60 min at 55.5 °C, while the EPR peak intensity of superoxide radical was lower at shorter reaction times. This was consistent with the trend of NO removal efficiency over time in the dual component of $Na_2S_2O_8/CaO_2$ solution at 55.5 °C. It was difficult to determine the presence of $SO_4^{\bullet-}$ and •OH radicals because the fluxes of $SO_4^{\bullet-}$ and •OH radicals were low in the dual component of $Na_2S_2O_8/CaO_2$ solution, or because the EPR peaks of $SO_4^{\bullet-}$ and •OH radicals were overlapped with that of $O_2^{\bullet-}$ radical [36]. The EPR peaks of $SO_4^{\bullet-}$ and •OH radicals were determined in the $Na_2S_2O_8$ solution at 55.5 °C.

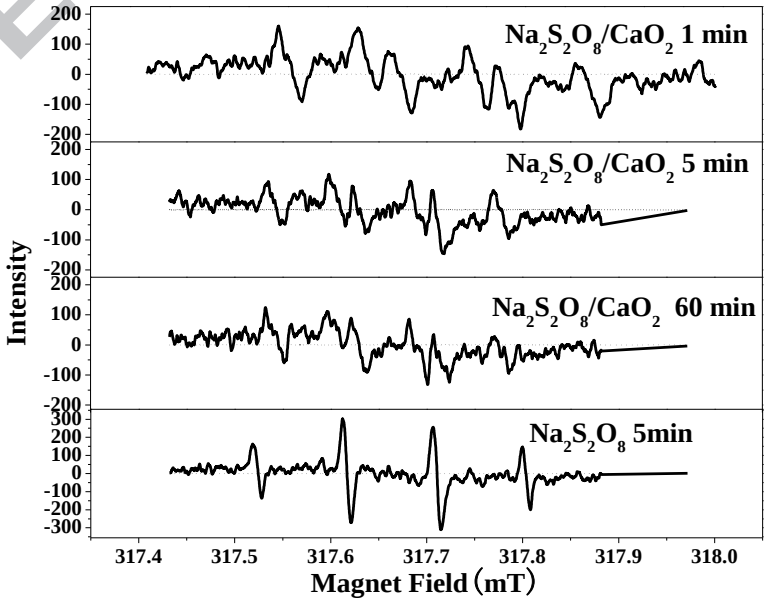

Fig. 14. EPR spectra of radical adducts in $Na_2S_2O_8$ solution and dual component of

$Na_2S_2O_8/CaO_2$ solution at 55.5 ℃.

The reaction mechanisms of NO removal by the dual component of $Na_2S_2O_8/CaO_2$ solution at 55.5 ℃ can be described as follows. In the single CaO_2 solution system, NO was mainly oxidized and absorbed by H_2O_2 and the $Ca(OH)_2$ released by CaO_2 (See Eqs. 7 and 24-27).

$$NO + H_2O_2 \rightarrow HNO_2 + H_2O \quad (24)$$

$$HNO_2 + H_2O_2 \rightarrow HNO_3 + H_2O \quad (25)$$

$$2HNO_2 + Ca(OH)_2 \rightarrow Ca^{2+} + 2NO_2^- + 2H_2O \quad (26)$$

$$2HNO_3 + Ca(OH)_2 \rightarrow Ca^{2+} + 2NO_3^- + 2H_2O \quad (27)$$

In the $Na_2S_2O_8$ solution system, NO was mainly oxidized and absorbed by $SO_4^{\bullet-}$ produced by the thermal activation of $Na_2S_2O_8$ (See Eqs. 8-9 and 28-29).

$$SO_4^{\bullet-} + NO + H_2O \rightarrow 2H^+ + SO_4^{2-} + NO_2^- \quad (28)$$

$$SO_4^{\bullet-} + NO_2^- + H_2O \rightarrow 2H^+ + SO_4^{2-} + NO_3^- \quad (29)$$

In the dual component $Na_2S_2O_8/CaO_2$ solution, NO was mainly oxidized and absorbed by $O_2^{\bullet-}$, $SO_4^{\bullet-}$ and •OH radicals generated thermally, activation of $Na_2S_2O_8$ by H_2O_2 and OH^- (See Eqs. 10-15 and 28-34) and $Ca(OH)_2$ released by CaO_2 (See Eqs 26-27, 35).

$$OH\cdot + NO \rightarrow H^+ + NO_2^- \quad (30)$$

$$NO_2^- + OH\cdot \rightarrow OH^- + NO_2 \quad (31)$$

$$NO_2 + OH\cdot \rightarrow H + NO_3^- \quad (32)$$

$$2O_2^{\bullet-} + 2NO \rightarrow O_2 + 2NO_2^- \quad (33)$$

$$2O_2^{\bullet-} + 2NO \rightarrow 2NO_3^- \quad (34)$$

$$SO_4^{2-} + Ca(OH)_2 + 2H_2O \rightarrow CaSO_4 \cdot 2H_2O + 2OH^- \quad (35)$$

4. Conclusions

We studied a wet NO_x removal technology using a $Na_2S_2O_8/CaO_2$ solution. The performance of the dual component $Na_2S_2O_8/CaO_2$ was stable at room temperature and atmosphere pressure. Comparative performance studies showed that the combination of $Na_2S_2O_8$ and CaO_2 had significant synergistic effects on NO removal. With an increase of CaO_2 concentration and reaction temperature, NO removal efficiency first rapidly increased and then slowed down. With the increase of initial pH, NO removal efficiency first increased and then decreased. NO removal efficiency did not show a significant relationship with $Na_2S_2O_8$ concentration or O_2 concentration. NO removal efficiency decreased almost linearly from 94.5 % to 75.1 % with the increase in NO concentration from 139 to 559 ppm. According to the EPR analysis, free radicals of $O_2^{\bullet-}$, $SO_4^{\bullet-}$ and •OH played a key role in the NO removal in the dual component of $Na_2S_2O_8/CaO_2$ solution. This will contribute to a better understanding of the reaction mechanisms of NO removal with $Na_2S_2O_8/CaO_2$.

Acknowledgements

This study was supported by the International S&T Cooperation Program of China (Grant No. 2015DFG61910).

References

1. Q. Wu, C.L. Sun, H.Q. Wang, T. Wang, Y.J. Wang, Z.B. Wu, The role and mechanism of triethanolamine in simultaneous absorption of NO_x and SO_2 by magnesia slurry combined with ozone gas-phase oxidation, Chem. Eng. J. 341

(2018) 157-163.

2. Y. Zhao, H. Wang, T.H. Wang, Adsorption of NO from flue gas by molecularly imprinted adsorbents, Chem. Eng. J. 306 (2016) 832-839.
3. W.Y. Sun, S.L. Ding, S.S. Zeng, S.J. Su, W.J. Jiang, Simultaneous absorption of NO_x and SO_2 from flue gas with pyrolusite slurry combined with gas-phase oxidation of NO using ozone, J. Hazard. Mater. 192 (2011) 124-130.
4. Z.H. Wang, J.H. Zhou, Y.Q. Zhu, Z.C. Wen, J.Z. Liu, K.F. Cen, Simultaneous removal of NO_x, SO_2 and Hg in nitrogen flow in a narrow reactor by ozone injection: Experimental results, Fuel Process. Technol. 88 (2007) 817-823.
5. Y.G. Adewuyi, N.Y. Sakyi, Simultaneous absorption and oxidation of nitric oxide and sulfur dioxide by aqueous solutions of sodium persulfate activated by temperature, Ind. Eng. Chem. Res. 52 (2013) 11702-11711.
6. Y.S. Mok, H.J. Lee, Removal of sulfur dioxide and nitrogen oxides by using ozone injection and absorption-reduction technique, Fuel Process. Technol. 87 (2006) 591-597.
7. M.M. Collins, C.D. Cooper, J.D. Dietz, C.A. Clausen, L.M. Tazi, Pliot-scale evaluation of H_2O_2 injection to control NO_x emissions, J. Environ. Eng-ASCE. 127 (2001) 329-336.
8. D.S. Jin, B.R. Deshwal, Y.S. Park, H.K. Lee, Simultaneous removal of SO_2 and NO by wet scrubbing using aqueous chlorine dioxide solution, J. Hazard. Mater. 135 (2006) 412-417.
9. P. Fang, C.P. Cen, X.M. Wang, Z.J. Tang, Z.X. Tang, D.S. Chen, Simultaneous

removal of SO_2, NO and Hg^0 by wet scrubbing using urea+$KMnO_4$ solution, Fuel Process. Technol. 106 (2013) 645-653.

10. Y. Zhao, T.X. Guo, Z.Y. Chen, Y.R. Du, Simultaneous removal of SO_2 and NO using M/$NaClO_2$ complex absorbent, Chem. Eng. J. 160 (2010) 42-47.
11. M.K. Mondal, V.R. Chelluboyana, New experimental results of combined SO_2 and NO removal from simulated gas stream by NaClO as low-cost absorbent, Chem. Eng. J. 217 (2013) 48-53.
12. N.E. Khan, Y.G. Adewuyi, Absorption and oxidation of nitric oxide (NO) by aqueous solutions of sodium persulfate in a bubble column reactor, Ind. Eng. Chem. Res. 49 (2010) 8749-8760.
13. Y.G. Adewuyi, M.A. Khan, Nitric oxide removal from flue gas by combined persulfate and ferrous–EDTA solutions: Effects of persulfate and EDTA concentrations, temperature, pH and SO_2, Chem. Eng. J. 304 (2016) 793-807.
14. X.L. Long, H.X. Cao, B.B. Duan, M.L. Jia, Removal of NO with the hexamminecobalt solution catalyzed by the carbon treated with oxalic acid, Environ. Sci. Pollut. Res. 24 (2017) 27788-27798.
15. C.D. Cooper, C.A. Clausen, L. Pettey, M.M. Collins, M.P. de Fernandez, Investigation of ultraviolet light-enhanced H_2O_2 oxidation of NO_x emissions, J. Environ. Eng-ASCE. 128 (2002) 68-72.
16. M.H. Nie, Y. Yang, Z.J. Zhang, C.X. Yan, X.N. Wang, H.J. Li, W.B. Dong, Degradation of chloramphenicol by thermally activated persulfate in aqueous solution, Chem. Eng. J. 246 (2014) 373-382.

17. T.K. Lau, W. Chu, N.J.D. Graham, The aqueous degradation of butylated hydroxyanisole by UV/$S_2O_8^{2-}$: study of reaction mechanisms via dimerization and mineralization, Environ. Sci. Technol. 41 (2007) 613-619.

18. Z.S. Wei, F.A. Villamena, L.K. Weavers, Kinetics and mechanism of ultrasonic activation of persulfate: an in situ EPR spin trapping study, Environ. Sci. Technol. 51 (2017) 3410-3417.

19. M.H. Nie, C.X. Yan, M. Li, X.M. Wang, W.L.Bi, W.B. Dong, Degradation of chloramphenicol by persulfate activated by Fe^{2+} and zerovalent iron, Chem. Eng. J. 279 (2015) 507-515.

20. H.Y. Liang, Y.Q. Z, S.B. Huang, I. Hussain, Oxidative degradation of p-chloroaniline by copper oxidate activated persulfate, Chem. Eng. J. 218 (2013) 384-391.

21. P.A. Block, R.A. Brown, D. Robinson, Novel activation technologies for sodium persulfate in situ chemical oxidatio, in Proceedings of the Fourth International Conference on Remediation of Chlorinated and Recalcitrant Compounds, 2004, Monterey, CA.

22. Z.P. Wang, Z.W. Wang, Reaction performance study on denitration in aqueous solution of the dual oxidant (H_2O_2/$S_2O_8^{2-}$), Environ. Prog. Sustain. 35 (2016) 1361-1366.

23. Z.P. Wang, Z.W. Wang, Y. Ye, N. Chen, H.W. Li, Study on the removal of nitric oxide (NO) by dual oxidant (H_2O_2/$S_2O_8^{2-}$) system, Chem. Eng. Sci. 145 (2016) 133-140.

24. R.L. Hao, S. Yang, B.Yuan, Y. Zhao, Simultaneous desulfurization and denitration through an integrative process utilizing $NaClO_2/Na_2S_2O_8$, Fuel Process. Technol. 159 (2017) 145-152.

25. A. Zhang, X. Shen, X.Y. Yin, X. Li, Y.N. Liu, Application of calcium peroxide for efficient removal of triamcinolone acetonide from aqueous solutions: Mechanisms and products, Chem. Eng. J. 345 (2018) 594-603.

26. D.A. House, Kinetics and mechanism of oxidations byperoxydisulfate, Chem. Rev. 62 (1962) 185-203.

27. A. Zhang, J. Wang, Y. Li, Performance of calcium peroxide for removal of endocrine-disrupting compounds in waste activated sludge and promotion of sludge solubilization, Water Res. 71 (2015) 125-139.

28. A. Fischbacher, J.V. Sonntag, C.V. Sonntag, T.C. Schmidt, The •OH radical yield in the H_2O_2 + O_3 (peroxone) reaction, Environ. Sci. Technol. 47 (2013) 9959-9964.

29. O.S. Furman, A.L. Teel, R.J. Watts, Mechanism of base activation of persulfate, Environ. Sci. Technol. 44 (2010) 6423-6428.

30. H.B. Jin, S.H. Yang, G.X. He, D.L. Liu, Z.M. Tong, Gas-liquid mass transfer characteristics in a gas–liquid–solid bubble column under elevated pressure and temperature, Chin. J. Chem. Eng. 22 (2014) 955-961.

31. R.L. Hao, Y.Y. Zhang, Z.Y. Wang, Y.P. Li, B. Yuan, X.Z. Mao, Y. Zhao, An advanced wet method for simultaneous removal of SO_2 and NO from coal-fired flue gas by utilizing a complex absorbent, Chem. Eng. J. 307 (2017) 562-571.

32. Y.X. Liu, Q. Wang, Removal of elemental mercury from flue gas by thermally activated ammonium persulfate in a bubble column reactor, Environ. Sci. Technol. 48 (2014) 12181-12189.

33. Y. Zhao, W. Qiu, C.Y. Yang, J.N. Wang, Study on a novel oxidation process for removing arsenic from flue gas, Energ. Fuel. 31 (2016) 693-698.

34. C.C. Chen, P.X. Lei, H.W. Ji, W.H. Wan, J.C. Zhao, Photocatalysis by titanium dioxide and polyoxometalate/TiO_2 cocatalysts. Intermediates and mechanistic study, Environ. Sci. Technol. 38 (2004) 329-337.

35. C. Xia, R. Fernandes, F.H. Cho, N. Sudhakar, B. Buonacorsi, S. Walker, M. Xu, J. Baugh, L.F. N, Direct evidence of solution-mediated superoxide transport and organic radical formation in sodium-oxygen batteries, J. Am. Chem. Soc. 138 (2016) 11219-11226.

36. A. Keszler, B. Kalyanaraman, N. Hogg, Comparative investigation of superoxide trapping by cyclic nitrone spin traps: the use of singular value decomposition and multiple linear regression analysis, Free. Radical. Bio. Med. 35 (2003) 1149-1157.

HIGHLIGHTS

- A novel wet method for NO removal with $Na_2S_2O_8/CaO_2$ as oxidants.
- Free radicals of $O_2^{\bullet-}$, $SO_4^{\bullet-}$ and •OH as the key species were identified by EPR.
- A better understanding of the reaction mechanisms of NO removal with $Na_2S_2O_8/CaO_2$.